



**HAL**  
open science

## Resilience improvement of an isotactic polypropylene-g-maleic anhydride by crosslinking using polyether triamine agents

Adrien Létoffé, Sandrine Hoppe, Richard M. Laine, Nadia Canilho, Andreea Pasc, Didier Rouxel, Rafael Jimenez Rioboo, Sebastien Hupont, Isabelle Royaud, Marc Ponçot

### ► To cite this version:

Adrien Létoffé, Sandrine Hoppe, Richard M. Laine, Nadia Canilho, Andreea Pasc, et al.. Resilience improvement of an isotactic polypropylene-g-maleic anhydride by crosslinking using polyether triamine agents. *Polymer*, 2019, 179, pp.121655. 10.1016/j.polymer.2019.121655 . hal-02276605

**HAL Id: hal-02276605**

**<https://hal.science/hal-02276605>**

Submitted on 25 Oct 2021

**HAL** is a multi-disciplinary open access archive for the deposit and dissemination of scientific research documents, whether they are published or not. The documents may come from teaching and research institutions in France or abroad, or from public or private research centers.

L'archive ouverte pluridisciplinaire **HAL**, est destinée au dépôt et à la diffusion de documents scientifiques de niveau recherche, publiés ou non, émanant des établissements d'enseignement et de recherche français ou étrangers, des laboratoires publics ou privés.



Distributed under a Creative Commons Attribution - NonCommercial 4.0 International License

# 1 Resilience improvement of an isotactic polypropylene-g- 2 maleic anhydride by crosslinking using polyether triamine 3 agents

4 Adrien Létouffé<sup>a,b</sup>, Sandrine Hoppe<sup>c</sup>, Richard Lainé<sup>c</sup>, Nadia Canilho<sup>d</sup>, Andreea Pasc<sup>d</sup>,  
5 Didier Rouxel<sup>a</sup>, Rafael J. Jiménez Riobóo<sup>e</sup>, Sébastien Hupont<sup>a</sup>, Isabelle Royaud<sup>a</sup>, Marc  
6 Ponçot<sup>\*a,b</sup>

7 <sup>a</sup>Université de Lorraine, CNRS, IJL, F-54000 Nancy, France

8 <sup>b</sup>Université de Lorraine, CNRS, LabEX "DAMAS", F-57000 Metz, France

9 <sup>c</sup>Université de Lorraine, CNRS, LRGP, F-54000 Nancy, France

10 <sup>d</sup>L2CM UMR CNRS 7053, Université de Lorraine, F-54506, Vandœuvre-lès-Nancy, France

11 <sup>e</sup>Instituto de Ciencia de Materiales de Madrid (CSIC), Sor Juana Inés de la Cruz, 3, E-28049, Madrid, Spain

12

---

## *Abstract:*

The elaboration of new hybrid polymer/metal composite materials depends on the development of innovative polymer matrices with improved mechanical properties and high effective adhesion behaviour with metal surfaces. This way, a new type of polyolefin was developed based on a peculiar crosslinking reaction. For this elaboration, an iPP-g-MAH with 1wt% of MAH was crosslinked with polyether triamine molecules by twin screw reactive extrusion. The evolution of the crosslinking reaction, the microstructure and the mechanical behaviour of the different materials were studied as a function of the NH<sub>2</sub>:MAH molar ratio in the range of 0:1 and 1.5:1. Gel content determination and FTIR analysis were performed to characterise the material at the molecular scale, when differential scanning calorimetry, wide angle X-rays scattering and self-successive auto-nucleation techniques were used for a deep microstructure analysis. Brillouin spectroscopy showed an interesting evolution of the elastic constants at the microscopic scale and results were in good agreement with those obtained at the macroscopic scale by a video-controlled uniaxial tensile test. Moreover, it was demonstrated that the true mechanical behaviours switch from brittle to ductile illustrating an important improvement of the resilience ability of the synthesized materials as a function of the NH<sub>2</sub>:MAH molar ratio even for molar ratio other than an equimolar ratio, with remaining MAH or NH<sub>2</sub> chemical groups for further chemical reaction.

*Keywords: isotactic polypropylene grafted maleic anhydride, polyether triamine, crosslinking, microstructure, molecular architecture, Brillouin spectroscopy, mechanical properties*

---

13

## 14 1. Introduction

15 The development of new multi-materials is an important topic of investigation that contributes  
16 to the reduction of ecological footprint of human activities. Furthermore, steel/polymer  
17 multilayer composites, used in different industrial applications, allow the generation of lighter  
18 structures. However, due to poor compatibility between the polymer and the metallic surface,  
19 processing is still being optimized. Since, functionalized polyolefins have adhesive properties  
20 that can promote for metal adhesion or nano-filler dispersion, they have been used either in  
21 blends with other polymers [1-3], or in the elaboration of polymer composites [4-6].

22 Polypropylene grafted with maleic anhydride (iPP-g-MAH), one of those classic functionalized  
23 polyolefins, is used in the elaboration of layered metallic/polymer composites. The main  
24 drawback of iPP-g-MAH is poor mechanical behavior due to the chain scissions that take place  
25 during the MAH grafting reaction [7-17]. In some cases, elastomer nodules are used to improve  
26 the mechanical properties of the polymer matrix [18]. Another type of functionalized  
27 polypropylene is polypropylene grafted with amine groups (iPP-g-NH<sub>2</sub>) usually produced from  
28 iPP-g-MAH by a grafting reaction of amino groups and the consumption of the MAH. The  
29 presence of amino groups change the properties of the polymer matrix. This may be reflected

30 in an increased ability to promote the exfoliation of silicate or graphene fillers [2, 4, 19].  
31 However, the mechanical properties of iPP-g-NH<sub>2</sub> remain low. The physical properties of the  
32 genuine iPP-g-MAH are mainly maintained.

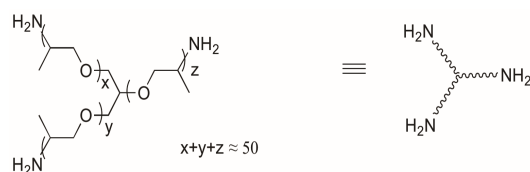
33 In the work reported here, the elaboration of a functionalized polyolefin matrix with significant  
34 shock absorption properties and free chemical groups, as MAH or NH<sub>2</sub>, has been investigated.  
35 The material generated is based on isotactic polypropylene grafted with maleic anhydride (iPP-  
36 g-MAH), which exhibits, as does classic polypropylene (PP), low price, low density and good  
37 processing ability. The chemical treatment used is based on a recently developed new  
38 crosslinking method for modification of the mechanical properties of different iPP-g-MAH  
39 [20].

40 This method was developed to overcome the detrimental effects of the maleic anhydride  
41 grafting reaction on the iPP polymer chains. The iPP-g-MAH, even at low MAH contents,  
42 display a brittle mechanical behaviour, with inefficient shock absorption properties. The  
43 crosslinking reaction was based on the reaction between maleic anhydride and the amino groups  
44 of a polyether diamine molecule [2, 19-22]. In previous work, two iPP-g-MAH at 1 and 3 wt %  
45 of MAH was crosslinked with a polyether diamine at different NH<sub>2</sub>/MAH molar ratios. The  
46 main results were a switch from brittle to ductile mechanical behaviour observed using video-  
47 controlled uniaxial tensile tests for the polymer obtained with an equimolar NH<sub>2</sub>:MAH molar  
48 ratio. In this situation, no MAH or amino groups remain free inside the matrix for further  
49 reaction. The aim of this new study was to use a polyether triamine in place of a common linear  
50 polyether diamine to always generate a three-dimensional macromolecular network, but  
51 permitting at the same time to reach interesting mechanical properties and ready-to-use free  
52 chemical functionality for molar ratios others than the equimolar one. The focus was led on  
53 molar ratios between amino and maleic anhydride groups from 0.33 to 1.5.

54 The reaction and the material structure were studied by infrared spectroscopy and determination  
55 of the gel proportion. The impacts of the reaction on the semi-crystalline microstructure were  
56 studied with the self-successive auto-nucleation technique (SSA) and X-ray scattering. The  
57 evolution of elastic constants and optical properties were studied using Brillouin spectroscopy  
58 and finally the VidéoTraction™ system was used to determine the true mechanical behaviour  
59 of the different materials.

## 60 2. Materials preparation

61 In this work, the crosslinking agent used was a polyether triamine distributed by Huntsman as  
62 the Jeffamine® T3000 [23] and used as received. The T3000 presents aliphatic polypropylene  
63 glycol (PPG) chains end capped by three amine groups and has a molecular weight of 3000  
64 g.mol<sup>-1</sup> (Fig. 1).



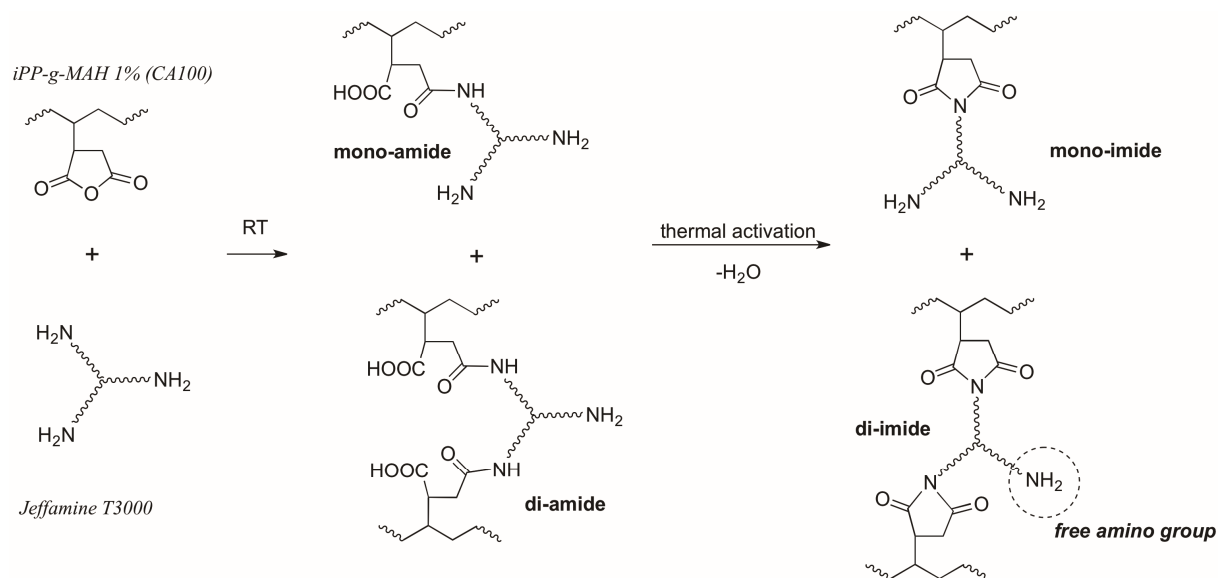
65  
66

**Fig. 1.** Molecular structure of the Jeffamine® T3000.

67 The T3000 polyether triamine is chemically more reactive toward maleic anhydride groups than  
68 aromatic amines [2].

69 The comparative polymer matrix used in this work is an isotactic polypropylene grafted with 1  
70 wt% of maleic anhydride, noted as CA 100 and distributed by Arkema under the commercial  
71 name, Orevac® CA 100. More information may be obtained from the Arkema specification  
72 sheet [24] or the previous paper [20]. It should be noted that the grafting process for MAH units  
73 involving peroxide molecules induces a significant decrease in the macromolecular mass of  
74 iPP. As a result, CA 100 shows a brittle mechanical behaviour.

75 The chemical reaction involved here, as shown in Fig. 2, is the reaction between MAH groups  
76 grafted on the polypropylene macromolecular chains and the T3000 amino groups. As a first  
77 step, the reaction between an amino group and a MAH group leads to the formation of an amide  
78 and a carboxylic acid. Then, at a much lower rate, cyclization to form an imide group occurs  
79 [1, 2, 19]. Previous analysis using FTIR spectroscopy has demonstrated that part of the  
80 amide/carboxylic acid pairs did not form an imide group in the final material [20]. It was also  
81 supposed that some MAH groups could react with two amines to form two amide groups [19].  
82 This situation is now considered unlikely since the carboxylic acid vibrational bands have  
83 remained at the same intensity in the excess material [20]. It is supposed that at an equimolar  
84 ratio, no MAH groups or free amino group are remaining.



85  
86 **Fig. 2.** Chemical reaction scheme illustrating the crosslinking steps between T3000 and iPP-g-MAH through the formation of  
87 either amide or imide units, with different final structures

88 The elaboration by reactive extrusion and the forming process by injection molding were  
89 carried out at the Reactions and Chemical Engineering Laboratory (LRGP) using a  
90 Thermofischer reactive extruder with exactly the same parameters as those used in previous  
91 work [20].

### 92 **3. Experimental methods:**

#### 93 **3.1. Gel Content determination:**

94 Gel content determination is a classic method for characterization of crosslinked polyolefins.  
95 In this work the ASTM D2765-84 standard method was used. The extraction solvent was  
96 boiling xylene and the test was carried out inside a copper pouch.

97 A square pouch made of copper is used to contain the sample, the pouch weight is noted  $W_1$ .  
98 The material sample of approximately 0.3 g is put inside the pouch. The weight of the pouch  
99 and the sample is noted  $W_2$ . The pouch is finally sealed and the weight is noted  $W_3$ . The sealed  
100 pouch is placed in boiling solvent for 8 hours, then dried at reduced pressure oven at 150°C for  
101 30 min. The final weight of the pouch is noted  $W_4$ . Finally, the solvent extraction is calculated  
102 as:

$$103 \quad E = \frac{W_3 - W_4}{(1 - F)(W_2 - W_1)} \times 100 \quad (1)$$

104  $F$  is the fraction filler in the polymer, insoluble in the xylene. The gel content is estimated at  
105  $100 - E$ . The measurements were performed at least three times to ensure the good  
106 reproducibility of results.

### 107 **3.2. Fourier Transform Infrared (FTIR) spectroscopy:**

108 FTIR analyses were performed at room temperature using an FTIR Magna Protégé 460 from  
109 Nicolet. The FTIR spectra were recorded from 400 to 4000  $\text{cm}^{-1}$  with a 4  $\text{cm}^{-1}$  resolution using  
110 an accumulation of 64 scans in the transmission mode. The samples were compressed at 190°C  
111 and 8 bars to form thin films between 100 and 200  $\mu\text{m}$ . The spectra were treated with the Fityk  
112 software and a reference band at 998  $\text{cm}^{-1}$ , which come from the methyl groups rocking, was  
113 used to normalize the overall spectral intensity.

### 114 **3.3. Wide angle X-rays Scattering (WAXS):**

115 The WAXS analyses were performed with a parabolic multilayer mirror (Osmic) and a  
116 cylindrical capillary. The selected wavelength is the copper radiation  $K\alpha_1$  ( $\lambda = 0.154 \text{ nm}$ )  
117 applied with a tension and an intensity of 30 kV and 40 mA. The samples are 1 cm by 1 cm  
118 square cut directly from the material sample and polished to remove any skin/core effect.

119 The 1D WAXS diffractograms presented reflect the average crystal diffraction in the sample  
120 plane. The effect of the potential crystalline texture was removed by the rotation of the sample  
121 holder. These diffractograms were analysed using the Hermans and Weidinger's method [25].  
122 A series of Gaussian and Lorentzian functions were used to fit the amorphous and crystalline  
123 phases contribution, respectively [26, 27]. The crystallinity ratio was estimated as the ratio of  
124 the crystalline peaks areas divided by the total area of the diffractogram.

125 The 2D WAXS patterns were obtained using a photosensitive plane film scanned using a  
126 FUJIFILM scanner BAS 5000. The sample was put at a distance of 75 mm from the film  
127 detector.

### 128 **3.4. Differential Scanning Calorimetry analysis (DSC):**

129 Calorimetric data were recorded using a Q200 TA Instruments apparatus. A 10 mg sample of  
130 each material were encapsulated with aluminium pans. The analyses were performed under an  
131 inert flux of azote atmosphere at a flow rate of 50  $\text{ml}\cdot\text{min}^{-1}$ . The samples were treated at a  
132 constant rate of 10°C·min<sup>-1</sup> (divide in heating, cooling, heating) from 30 to 200°C. The

133 crystallinity ratios of the different materials were estimated from the melting enthalpy ( $\Delta H_m$ )  
134 as follows:

$$135 \quad X_c = \frac{\Delta H_m}{\Delta H_m^0} \quad (2)$$

136  $\Delta H_m^0 = 165 \text{ J} \cdot \text{g}^{-1}$  is the enthalpy of a 100% crystalline isotactic polypropylene [28].

137 The main crystalline lamellar thickness population ( $L_c$ ) of the polymer is calculated from the  
138 Gibbs-Thomson equation:

$$139 \quad T_m = T_m^0 \left( 1 - \frac{2 \sigma_e}{\rho_c \Delta H_m^0 L_c} \right) \quad (3)$$

140 where the melting peak temperature  $T_m$  is estimated from the materials endotherms,  $T_m^0$  is the  
141 theoretical melting temperature of a 100% crystalline isotactic polypropylene given equal to  
142 460 K,  $\sigma_e$  is the surface free energy of iPP crystalline lamellae at  $0.0496 \text{ J} \cdot \text{m}^{-2}$  and  $\rho_c$  the  
143 crystalline phase density at  $0.9361 \text{ g} \cdot \text{cm}^{-3}$  [28, 29].

### 144 **3.5. Successive Self-Nucleation and Annealing (SSA):**

145 The Successive Self-Nucleation and Annealing experiments (SSA) is an experimental  
146 technique for characterization of the thickness distribution of crystalline lamella of a polymer  
147 [30, 31]. This technique based on the thermal fractionation of a semi crystalline polymer shows  
148 the linearity defects in the macromolecular chains, as co-monomers, stereo-defects or  
149 crosslinking [32]. This technique is used to study the decrease of the main lamellar thicknesses  
150 of a polymer as a function of its crosslinking degree [20, 33]. A SN protocol (self-nucleation)  
151 was first performed to identify the ideal self-nucleation temperature  $T_s$  of the material. Once  $T_s$   
152 was determined, the SSA protocol was carried out.

### 153 **3.7. Uniaxial tensile tests:**

154 The VidéoTraction™ system was used to characterise the true mechanical behaviours of the  
155 different materials of this study [18, 34-37]. The shape of the samples was dumb-bell type  
156 specimen with a geometrical defect in the middle of the useful zone. This defect ensures the  
157 localization of the plastic deformation (necking) where the video measurements were  
158 performed. A specific Representative Volume Element (RVE) was then defined by a seven dot  
159 markers pattern applied to the probe surface.

160 The axial true strain noted  $\epsilon_{33}$  was estimated by a polynomial interpolation of the markers  
161 displacement using Lagrange Transform and following Hencky's strain theory. In the case of  
162 uniaxial tensile testing, the two transversal strains,  $\epsilon_{11}$  and  $\epsilon_{22}$ , were estimated equal (the strain  
163 field is supposed transversally isotropic at the middle of the neck) [38-42]. All the mechanical  
164 analyses were performed at  $20^\circ\text{C}$  with a constant true strain rate of  $5.10^{-3} \text{ s}^{-1}$ . This rate was  
165 chosen because it ensures the perfect control of the constant true strain rate of the testing  
166 machine, and suppress the risk of self-heating from the deformation [41, 42].

167 The volume strain  $\epsilon_v$  in the RVE is calculated from the trace of the true strain tensor:

$$168 \quad \epsilon_v = \epsilon_{11} + \epsilon_{22} + \epsilon_{33} \quad (4)$$

169 When the volume strain is positive, it is called volume damage since the “reversible” elastic  
170 part can be neglected.

171 The axial true stress (Cauchy stress) is determined in the RVE as:

$$172 \quad \sigma_{33} = (F/S_0) * e^{-2\varepsilon_{11}} \quad (5)$$

173 with  $S_0$  is the initial cross-section at the RVE of the sample.

### 174 **3.8 Brillouin Spectroscopy:**

175 Brillouin Scattering spectroscopy (BS), like Raman spectroscopy, is a light scattering  
176 technique, providing direct information on the acoustic phonons of the material i.e. on collective  
177 oscillations of atoms and on the propagation of acoustic waves in the material, and therefore on  
178 the mechanical properties of the material. It avoids direct contact of the sample, which may be  
179 crucial for many experiments. It is remarkably well adapted to study soft materials [43, 44],  
180 since the opto-mechanical coupling between photons and acoustic phonons is then much more  
181 important than for hard materials [43], except in the case of induced phonons [45].

182 Therefore, BS provides noninvasive measurement of acoustic and elastic properties of  
183 oligomers [46, 47], polymers [48] and polymer nanocomposites [49-53]. In the scattered light,  
184 the interaction between the photons of the incident beam and the acoustic phonons in material,  
185 which occur at hypersonic frequencies (10 MHz – 100 GHz), leads to specific frequency shifts  
186 ( $f$ ) of the scattered laser light. Two conservation laws are followed by the photons and the  
187 phonons involved in the scattering process: conservation of energy, involving the frequencies  
188 of the incident and scattered light and of the acoustic wave (5), and conservation of momentum,  
189 which involves the light wave vectors and the acoustic wave vector  $q$  (6):

$$190 \quad \hbar\omega_s = \hbar\omega_i \pm \hbar\Omega \quad (6)$$

$$191 \quad \hbar k_s = \hbar k_i \pm \hbar q \quad (7)$$

192 As in Raman spectroscopy, Stokes/anti-Stokes scattering occurs, corresponding to the creation  
193 or annihilation of a phonon, hence the  $\pm$  signs. Assuming a negligible acoustic attenuation, the  
194 relation between the sound velocity  $v$ , the acoustic phonon frequency  $f$  and its wave vector  $q$   
195 can be calculated using equations (5) and (6):

$$196 \quad v = \frac{2\pi f}{q} = \frac{\lambda_0 f}{2n \sin\left(\frac{\theta_i}{2}\right)} \quad (8)$$

197 where  $\lambda_0$  is the laser wavelength, and  $\theta_i$  the angle between the incident and scattered wave  
198 vectors  $\vec{k}_i$  and  $\vec{k}_s$ . From which is obtained the elastic modulus, related to the sound velocity  
199 and the mass density  $\rho$  of the medium:

$$200 \quad c(\vec{q}) = \rho * v^2(\vec{q}) \quad (9)$$

201 The Brillouin spectroscopy were performed in a 90A geometry to obtain the transmission mode  
202 ( $f_{90A}$ ). The samples were obtained by microtomy cuts to produce a 20  $\mu\text{m}$  thin element put  
203 between two glass slides [44]. The reflection of the laser on the second blade leads to  
204 simultaneously backscattering mode acquisitions ( $f_{180}$ ) [44], and then enable to obtain the  
205 phononic frequencies  $f_{90A}$  and  $f_{180}$  in the same spectrum.

206 In this configuration, the equation (8) can be simplified as:

207 
$$V_{90A} = f_{90A} \frac{\lambda_0}{\sqrt{2}} \quad (10)$$

208 
$$V_{180} = f_{180} \frac{\lambda_0}{2*n} \quad (11)$$

209 
$$n = \frac{f_{180}}{\sqrt{2}*f_{90A}} \quad (12)$$

210 From which we can deduce in particular the optical index of the material noted n [44], besides  
211 the elastic constant. The reproducibility of our tests was done by checking different samples.

212 The longitudinal phonon mode which gives rise to the elastic constant  $c_{11}$  was observed, defined  
213 by the first elasticity tensor constant in the Hooke's law. This elastic constant is calculated with  
214 the equation (9) from:

215 
$$c_{11} = \rho * v_{90A}^2 \quad (13)$$

### 216 **3.9. Scanning Electron Microscopy:**

217 Scanning electron microscopy (SEM), like in our previous work, is used to analyse the fracture  
218 surface of the mechanical analysis samples. The SEM micrographies enlighten the differences  
219 between the mechanical behaviours, and the switch from a brittle to a ductile material. *Post*  
220 *mortem* micrographies were recorded with an environmental Quanta FEG 650 electron  
221 microscope from the FEI Company. The parameters selected were a pressure of 100 Pa of water  
222 vapour and a 4 kV acceleration voltage.

## 223 **4. Results and discussion:**

### 224 **4.1. Study of the crosslinking reaction:**

225 The gel content evolution, as a function of the NH<sub>2</sub>:MAH molar ratio, is shown in Fig. 3. The  
226 gel content shows an increase with NH<sub>2</sub>:MAH ratio from the unmodified material to the 1:1  
227 molar ratio material. The CA 100 unmodified shows 0% of gel content. This null value is logical  
228 due to the low molecular weight, consequence of the MAH grafting reaction and was already  
229 seen before [7-17, 20]. The increase of the gel content observed is then attributed to the  
230 crosslinking reaction of the polymer chains. The crosslinking reaction, with the use of polyether  
231 triamine, induces a three dimensional molecular network. The gel content stabilizes for the 1:1  
232 and the 1.5:1 molar ratio. This evolution was expected, and is similar to the material obtained  
233 using polyether diamine [20]. The difference with polyether diamine is, in this situation of  
234 amino groups in excess (1.5:1), part of the polyether triamine molecule reacts with two MAH  
235 groups and maintained the 3D network.

236 This effect of amine excess was observed in previous work with high NH<sub>2</sub>:MAH molar ratios  
237 [7-17], but also in the case of polyether diamine [20].

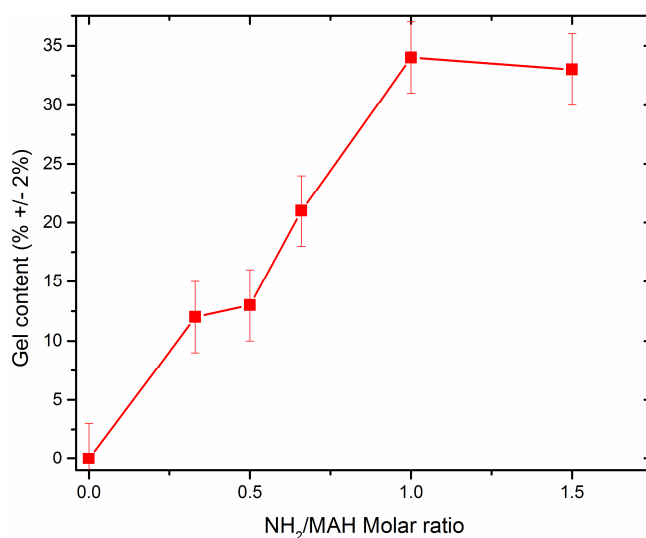


**Fig. 3.** Gel content measurements evolution as a function of the NH<sub>2</sub>:MAH molar ratio.

238

239

240 The FTIR analyses were performed to study the chemical evolution of the materials. The results  
 241 between 1900 and 1500 cm<sup>-1</sup> are presented in Fig. 4. For the unmodified CA 100 spectra, three  
 242 vibrational bands are observed, at 1860, 1780 and 1715 cm<sup>-1</sup>. The first two bands are assigned  
 243 to the symmetric and asymmetric ν<sub>C=O</sub> vibrations of the maleic anhydride group, and the third  
 244 one to the ν<sub>C=O</sub> vibrations, associated with carboxylic groups. The carboxylic acids must be  
 245 formed by hydrolysis of the maleic anhydride groups under wet storage conditions. Those three  
 246 bands intensities decrease with the NH<sub>2</sub>:MAH molar ratios, and, as expected, disappear at the  
 247 1:1 ratio.

248 Four other bands that appeared for the 0.33:1 material and reach a maximum at the 1:1 prove  
 249 the presence of imide and amide groups. First, two bands at respectively 1770 and 1700 cm<sup>-1</sup>  
 250 can be assigned to the symmetric and asymmetric ν<sub>C=O</sub> vibrations of the imide group, and two  
 251 others at 1735 and 1650 cm<sup>-1</sup> can be assigned to associated carboxylic acid/amide bonds. Those  
 252 bands confirmed the reaction between the MAH groups and the amino groups of the T3000.  
 253 The presence of amide/carboxylic acid bonds at 1735 and 1650 cm<sup>-1</sup> indicated an incomplete  
 254 imidization, as seen in previous report [20]. Those four bands stay at the same level of intensity  
 255 for the 1.5:1 ratio, the excess of amino group did not stop the reaction, but a new band at 1550  
 256 cm<sup>-1</sup> is observed. This band is assigned to primary amino groups that did not react. Those bands  
 257 evolution is consistent with the chemical reaction that takes place during the extrusion process  
 258 [1, 2, 19-22].

259 This evolution, with a complete use of amino groups for the materials between 0.33:1 and 1:1,  
 260 and the disappearance of MAH groups for the 1:1 molar ratio confirmed the complete extent of  
 261 the reaction for this specific ratio. The amino bands found for the 1.5:1 material, which  
 262 characterized the excess of crosslinking agent, is also in agreement with this. As seen as gel  
 263 content evolution shows in Fig. 3.

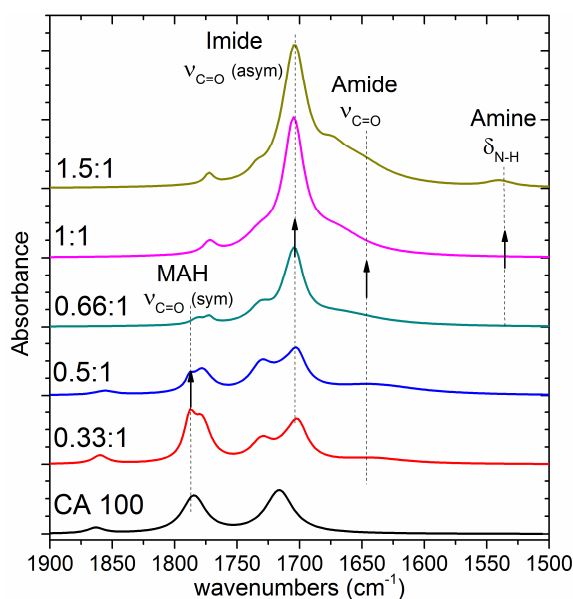


Fig. 4. Evolution of the FTIR spectra as a function of the MAH: NH<sub>2</sub> molar ratio.

264  
265

266 The gel content determination and the FTIR results confirmed a chemical and structural  
267 modification of the CA 100 by the T3000, close to the evolution observed before [20]. The  
268 reaction, proved by the FTIR results, create a three-dimensional molecular network. These  
269 structures evolution should influence the macromolecules mobility and/or the semi-crystalline  
270 microstructure of the materials, and may finally modify their mechanical behaviours.

#### 271 **4.2 Microstructural evolution**

272 The impact of a crosslinking reaction on the semi-crystalline structure because of the three-  
273 dimensional network can change a lot depending on the reaction. In the case of the MAH/NH<sub>2</sub>  
274 grafting reaction used in this work that takes place in melt state, previous studies showed a  
275 diminution of the lamellar thickness with the NH<sub>2</sub>:MAH ratio for the iPP-g-MAH at 1 wt% of  
276 MAH content [20]. To investigate these effects for these new materials crosslinked *via* the  
277 T3000 one-dimensional WAXS and DSC experiments were performed.

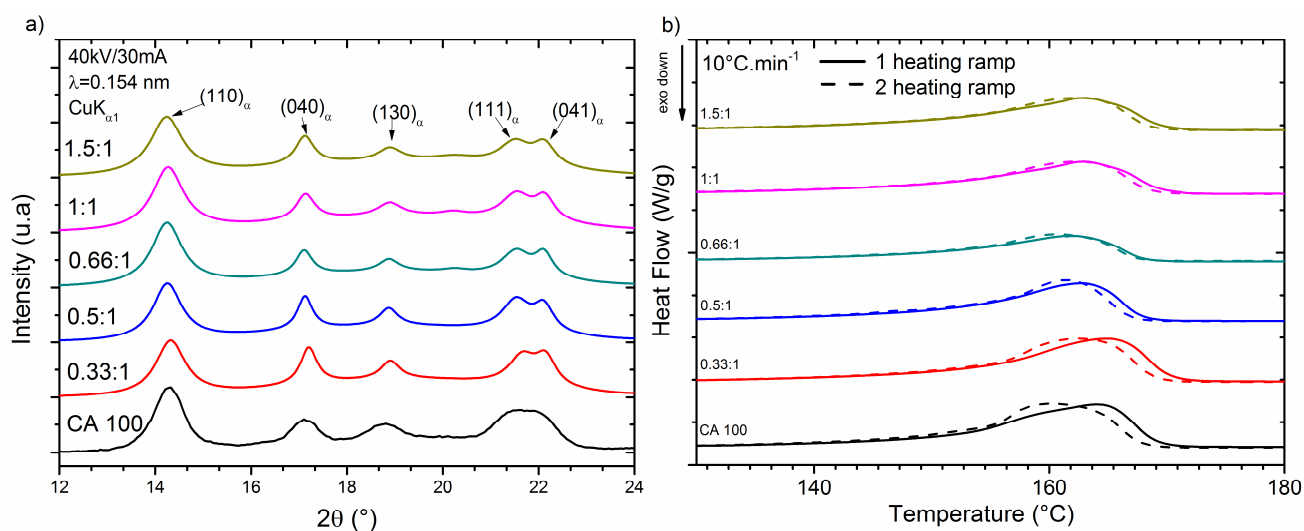


Fig. 5. a) 1D WAXS diffractograms and b) DSC thermograms evolution as a function of the NH<sub>2</sub>:MAH molar ratio.

278  
279

280 Fig. 5 a) shows the 1D WAXS results. Those diffractograms highlight the presence of the  
 281 monoclinic  $\alpha$  crystalline phase of the iPP in majority [53, 54] but also a small amount of the  $\beta$   
 282 crystalline phase. The  $\beta$  phase was neglected since it represents less than 1% of the crystalline  
 283 structure. No significant shift of the diffraction peak positions and no modification of the  
 284 crystallinity ratio was induced with the increase of the NH<sub>2</sub>:MAH molar ratio.

285 The DSC thermograms of the different materials are presented on Fig. 5 b). For all samples,  
 286 large endotherms around 160°C could be assigned to the melting of  $\alpha$  crystalline phase of iPP.  
 287 The maximum peaks associated with the main melting temperature  $T_m$  and the crystallinity  
 288 ratios are given for the first and second endotherms in Table 1. The crystallinity ratios between  
 289 the first and the second heating ramp remain close for all the materials with a maximum gap of  
 290 2%; this value is inferior to the experimental error. The same observation can be done between  
 291 the different materials with the maximum gap of 3%. The values of the crystallinity ratios  
 292 determined from WAXS analyses and deduced from the endotherm areas of the DSC first  
 293 heating ramp are significantly different but put in evidence the same tendency towards the  
 294 chemical reaction advancement. The two experimental techniques give results that cannot be  
 295 compared in absolute values for a specific material, but it is relevant to compare their trends. In  
 296 the two cases only small variations of crystallinity ratio appeared with the rise of the NH<sub>2</sub>:MAH  
 297 molar ratio. The crosslinking reaction does not induce significant modification of the  
 298 crystallinity ratio as compared to the unmodified CA 100.

299 This evolution is quite similar to the one observed with the same iPP-g-MAH modified with  
 300 polyether diamine [20]. Only a slight decrease of the main melting temperature can be observed  
 301 between the two heating ramps. There is certainly an influence of the injection on the  
 302 microstructure. This difference is maximal for the unmodified material and the 0.33:1 material  
 303 and decreases for higher NH<sub>2</sub>:MAH molar ratio. A double shoulder shaped endotherms is  
 304 observed for materials under the 0.5:1 molar ratio. For the unmodified CA 100 material, the  
 305 main crystalline population appears to be the one at the highest melting temperature for the first  
 306 endotherms, but switch to the lowest one for the second. For the 0.33:1 material, the main  
 307 crystalline population remains the same between the two endotherms. Also, a slight rise of the  
 308 melting temperature is observed between the unmodified CA 100 and the 0.33:1 material, from  
 309 163 to 165°C for the first heating ramp, and from 161 to 164°C for the second heating ramp.  
 310 The evolution of the two crystalline population rise was unexpected compared to previous  
 311 results, and indicates a small nucleation effect at low level of crosslinking. This effect seems to  
 312 counteract at higher molar ratio. The first heating endotherms show a decrease of the main  
 313 melting temperature from 165 to 163°C from the 0.33:1 to the 0.5:1 molar ratio, and finally  
 314 decreases to 161°C for the equimolar ratio. For the 1.5:1 NH<sub>2</sub>:MAH molar ratio, this effect  
 315 disappears, probably due to the presence of unreacted T3000 molecules, that tend to facilitate  
 316 the chain mobility.

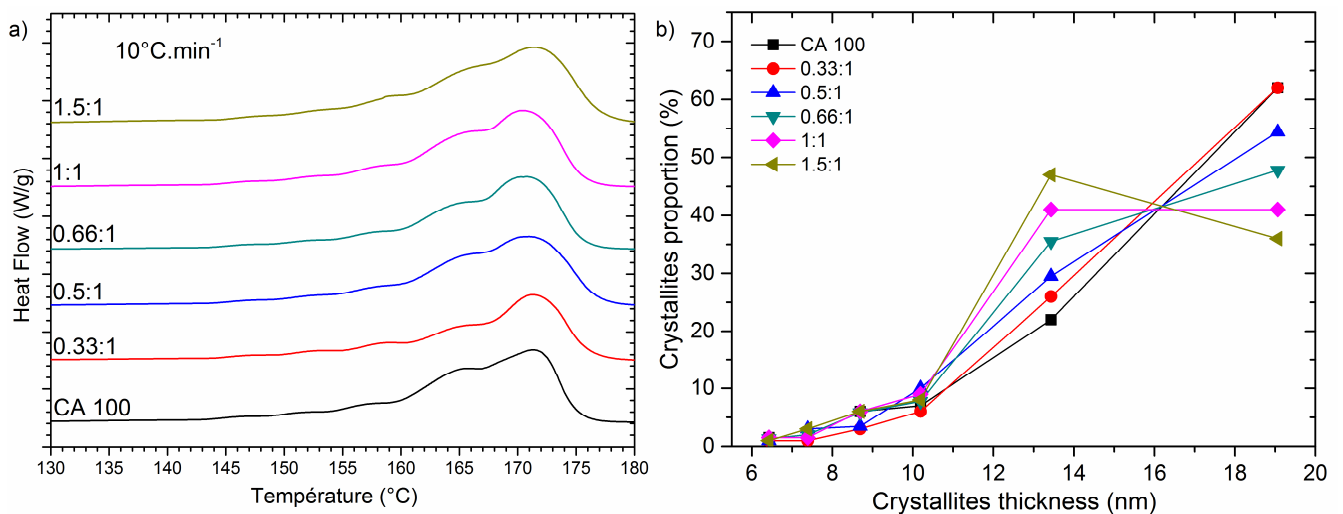
317 **Table 1**

318 Evolution of the crystallinity ratio and melting temperatures as function of the NH<sub>2</sub>:MAH molar ratio.

Materials	unmodified	0.33:1	0.5:1	0.66:1	1:1	1.5:1
$X_c (\pm 3\%) (1^{st} \text{ heating})$	45	46	47	47	44	44
$T_m (\pm 1^\circ\text{C})(1^{st} \text{ heating})$	165/160	165/161	163	162	161	162
$X_c (\pm 3\%)(2^{nd} \text{ heating})$	47	45	47	46	44	44
$T_m (\pm 1^\circ\text{C})(2^{nd} \text{ heating})$	161	164/163	161	160	161	161
$X_c (\pm 3\%)(1\text{D WAXS})$	62	59	60	62	61	61

320

321 The diminution of the melting temperatures implies, with the Gibbs-Thomson relation  
 322 (Equation 2), a fall of the crystalline lamellae thicknesses, from 13 nm for the 0.33:1 material  
 323 to 11 nm for the 1:1 material. It is assumed that the crosslinked part of the material is located  
 324 in the amorphous phase and does not alter the crystalline phase characteristics such as  
 325 monoclinic cell parameters, crystalline density and crystallites surface energy. The crosslinked  
 326 network created by the reaction shows an impact on the crystallisation of the material which is  
 327 small compared to other crosslinking methods [21, 22, 56-58]. To properly highlight the impact  
 328 of the reaction and the molar ratio on the melting temperature ranges for the modified samples  
 329 SN/SSA studies were performed. To start the SSA protocol, an SN protocol was performed on  
 330 the material with the higher melting temperature (0.33:1). The  $T_s$  temperature were determined  
 331 at 170°C for the 0.33:1 molar ratio.



332

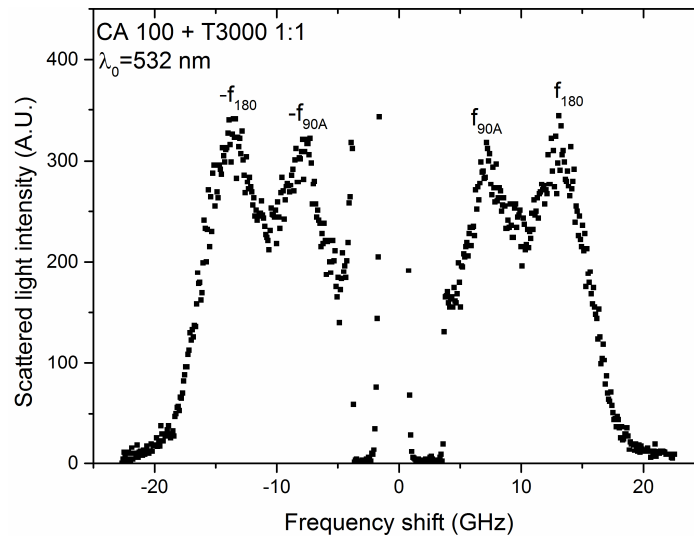
333 **Fig. 6.** a) SSA last thermograms for the different materials as a function of the NH<sub>2</sub>:MAH molar ratio, and b) distribution of  
 334 the different lamellae populations between the different thickness according to their melting temperature.

335 Fig. 6 shows the final heating ramp of the SSA protocol for the materials from the unmodified  
 336 CA 100 to the 1.5:1 material (Fig 6 a)), and the repartition of the crystallinity between the  
 337 different crystallite size population (Fig 6 b)). Six different crystalline lamellae populations  
 338 appear for each material. No change appeared for the first thickest crystallites ( $L_c = 19.5$  nm)  
 339 between the unmodified CA 100 and the 0.33:1 material, whereas the second thickest ones ( $L_c$   
 340 = 15.5 nm) present a rise from 22 to 26% of the crystallinity ratio. This rise explains the  
 341 evolution of the melting temperature between the two materials, and the evolution of the double  
 342 shoulder shaped endotherms. The reaction, at low levels of crosslinking, impacts positively the  
 343 crystallisation of the medium chain elements of the polypropylene and implied the rise of the  
 344 melting temperature observed by DSC analysis. For the highest molar ratios from the 0.5:1  
 345 material, a fall of the thickest crystalline population associated with the longest chain elements  
 346 is observed, from 62% for the unmodified CA 100 and the 0.33:1 material to 55% for the 0.5:1  
 347 material and 41% for the 1:1 molar ratio. This decrease is in favour of the second thickest  
 348 population associated to the medium chain elements, which represents 41 % of the 1:1 material  
 349 crystallinity. The crosslinking reaction, with the creation of chemical network, affects the  
 350 crystallisation of the longest chain elements. This evolution explains the decrease of the melting  
 351 temperature observed by DSC. The microstructure evolution observed with the increase of the  
 352 NH<sub>2</sub>/MAH molar ratio is similar to the previous results obtained with similar method [20], or  
 353 in case of other crosslinked polymers in the literature, but at a smaller scale [21, 22, 56-58].

354 The small rise of melting temperature for the 0.33:1 material, in correlation with the SSA  
355 protocol results, indicates a small nucleation effect of T3000 that was not previously observed  
356 [20]. This effect looks counterbalanced at higher molar ratio by the three-dimensional network  
357 formation, with a slight decrease of the melting temperatures ranges, as pointed out by SSA  
358 results.

### 359 4.3 Mechanical and optical properties evolution

360 To analyse the evolution of the mechanical behaviour of the different materials with the  
361 crosslinked reaction, Brillouin spectroscopy and VidéoTraction™ tests in uniaxial tension  
362 deformation path were performed. Fig. 7 presents a typical Brillouin response in case of CA  
363 100 1:1.



364

365

**Fig. 7.** Typical Brillouin response of the the 1:1 NH<sub>2</sub>:MAH molar ratio crosslinked polypropylene.

366 As expected, the two frequencies  $f_{90A}$  and  $f_{180}$  of the acoustic phonon were obtained. Fig. 8.  
367 present the evolution of the elastic modulus ( $c_{11}$ ) and refractive index ( $n$ ) for the different  
368 materials, considering a constant material density to within 0.905. The elastic modulus shows  
369 a rise from the unmodified materials to the 1:1 molar ratio, with 26% augmentation from 9.9 to  
370 12.5 GPa, and finally falls to 11.5 GPa for the 1.5:1 molar ratio. The evolution is consistent  
371 with previous results, and was expected in particular from the plasticizing effect of the polyether  
372 triamine for molar ratio higher than the 1:1.

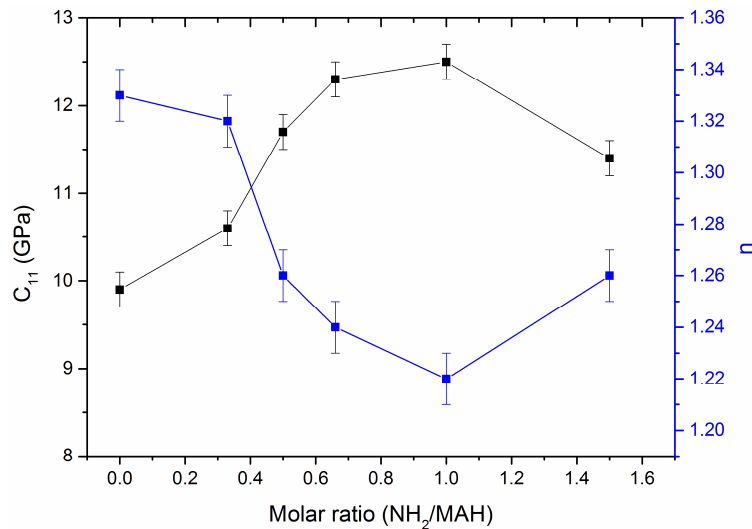


Fig. 8.  $C_{11}$  elastic constant and refractive index  $n$  evolution as a function of the  $\text{NH}_2$ :MAH molar ratio.

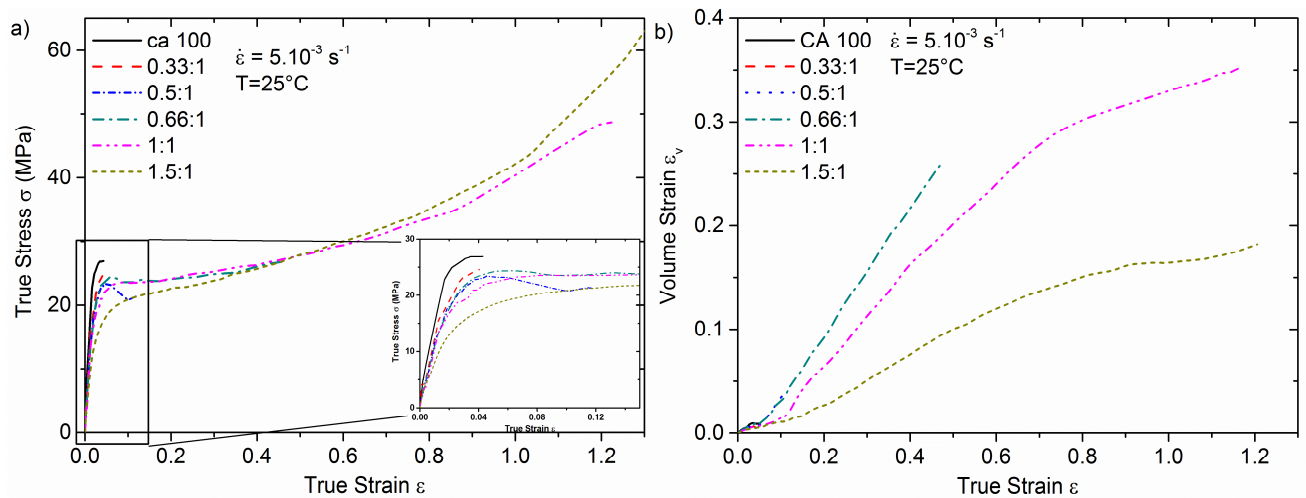
373  
374

375 This evolution can be easily explained by the creation of the crosslinked network inside the  
 376 materials by the T3000. As seen by FTIR analysis and gel content, this network depends on the  
 377 molar ratio, and shows no important evolution above the 1:1 molar ratio. This network does not  
 378 present an important impact on the crystalline phase, as discussed earlier in the microstructure  
 379 part, and remains located inside the amorphous phase. This network implied a stiffening of the  
 380 amorphous phase and the rise of elastic properties. For the 1.5:1 molar ratio, the unreacted  
 381 amine groups from the T3000 act like a plasticizer agent.

382 Furthermore, one expects a close correlation between mechanical and optical properties and in  
 383 the particular case of these materials, there is a symmetrical look of both curves (it is clear from  
 384 eq.12 that the frequency  $f_{90A}$ , which shows the greatest variation, controls the evolution of the  
 385 optical index): the higher the elastic constant, the lower the optical index. Interesting is to notice  
 386 that this effect is not universal and for instance in Phosphate glasses, among others, the higher  
 387 the Young's modulus the higher the refractive index [59].

388 To highlight the impact of the reaction on the true mechanical behaviour of the materials,  
 389 VidéoTraction™ tests in uniaxial tension deformation path were performed on the different  
 390 material at a constant true strain rate of  $5.10^{-3} \text{ s}^{-1}$ . Fig. 9 shows the true mechanical behaviours  
 391 of the different materials, with the evolution of the true stress and the volume strain as a function  
 392 of the true strain. As seen before, the iPP-g-MAH unmodified (CA 100) shows a brittle  
 393 mechanical behaviour [20]. The 0.33:1 material, the one with the lowest crosslinking level, also  
 394 presents a brittle behaviour. In this situation, the three-dimensional network seems not enough  
 395 to affect positively the mechanical properties of the material. The first main change appears for  
 396 the 0.5:1 material, with a true strain at break that rises from  $\epsilon_{b \text{ CA100}} = 0.04$  to  $\epsilon_{b \text{ 0.5:1}} = 0.12$ .  
 397 With the use of a polyether triamine, a switch from brittle to ductile mechanical behaviour starts  
 398 from the 0.5:1 molar ratio. This evolution appears clearly for the 0.66:1 material, with a strain  
 399 at break of  $\epsilon_{b \text{ 0.66:1}} = 0.45$ , but no modification of the level of true stress at break ( $\sigma_{b \text{ CA100}} = 26$   
 400 MPa and  $\sigma_{b \text{ 0.66:1}} = 27$  MPa). The rise of true strain at break continues for the equimolar material,  
 401 with also a modification of the true stress at break twice higher than the unmodified material  
 402 ( $\epsilon_{b \text{ 1:1}} = 1.22$  and  $\sigma_{b \text{ 1:1}} = 49$  MPa). This evolution is easily explained by the three dimensional  
 403 network highlighted by the rise of the gel content. The 1.5:1 material that presents an excess of  
 404 amino group shown by the FTIR, presents also a ductile behaviour with a diminution of the true  
 405 stress level at the beginning of the plastic deformation compared with the 1:1 material. It also

406 presents a more important amplitude of its stress hardening ( $\epsilon_{b\ 1.5:1} = 1.3$  and  $\sigma_{b\ 1.5:1} = 63$  MPa)  
 407 that could be explained by a higher level of molecular chain orientation towards the stretching  
 408 direction. This final evolution between the 1:1 and 1.5:1 material was unexpected, due to  
 409 previous results obtained with polyether diamine [20]. In the previous work the excess of amino  
 410 group presents a plasticizing effect with a diminution of true stress level. This evolution of  
 411 mechanical properties is in perfect correlation with the previous result like the gel content  
 412 determination and Brillouin spectroscopy. It is important to note that due to the brittle  
 413 mechanical behavior of the unmodified material (CA100), and the low ductility profile of the  
 414 materials with the lowest molar ratios, the calculation of the Young moduli, by the slope of the  
 415 elastic part of the VidéoTraction™ system curves, is difficult and exhibits a high level of  
 416 uncertainty. Moreover, due to the slight differences observed at low frequencies, Dynamical  
 417 Mechanical Thermal Analysis are so much relevant. These two reasons justify the use of  
 418 Brillouin spectroscopy.



419

420

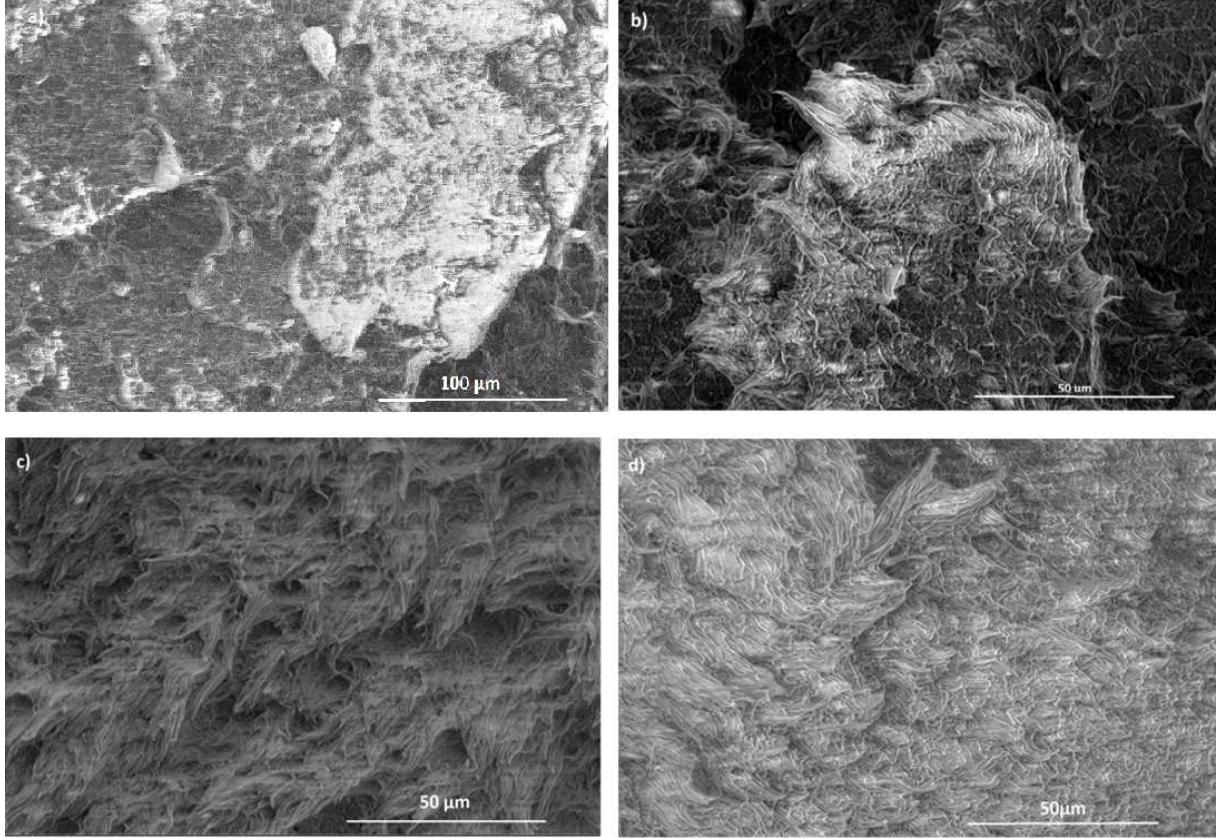
421

**Fig. 9.** Evolution of the a) true mechanical behaviour and  
 b) volume strain in uniaxial tension for the different crosslinked materials.

422 The change of volume strain with the molar ratio indicates that a complete reaction (1:1 molar  
 423 ratio) induces a fall of volume strain at the same level of true strain. The excess of amino groups  
 424 also decreases it, with a volume strain at break twice lower than the 1:1 material ( $\epsilon_{vb\ 1:1}=0.35$   
 425 and  $\epsilon_{vb\ 1.5:1}=0.18$ ). This fall is in good agreement with the highest level of molecular chain  
 426 orientation supposed from the true mechanical behaviour and the most important amplitude of  
 427 its stress hardening observed for the 1.5:1. For this material, the FTIR analysis confirmed the  
 428 complete extent of the reaction, with the total disappearance of the MAH bands and the presence  
 429 of unreacted amino groups. However, the close values of gel content between the 1:1 and 1.5:1  
 430 materials indicate the same level of crosslinking. In this configuration each polyether triamine,  
 431 statistically reacts with two different MAH groups and has one free branch with an unreacted  
 432 amino group. Here, due to the important size of each free branches ( $1000\text{ g}\cdot\text{mol}^{-1}$ ) the three  
 433 dimensional network is denser compared with the 1:1 material that induces the difference of  
 434 the true mechanical behaviours.

435 SEM micrographies of the fractured surface of the different stretched materials are given in Fig  
 436 10. In Fig 10 a), the unmodified CA 100 micrography indicates a brittle behaviour with no  
 437 plastic deformation. Fig 11 b) presents the heterogeneous surface of the 0.5:1 material. It put in  
 438 evidence the creation of a fibrillar microstructure distributed amongst some brittle zones that

439 confirms the transition of mechanical behaviour around this molar ratio. This evolution is  
 440 completed for the 1:1 molar ratio as seen in the Fig 10 c), with a complete fibrillar  
 441 microstructure that is conform to the complete switch of mechanical behaviour observed by the  
 442 tensile test results. Finally, the structure is maintained for the 1.5:1 material, the excess of  
 443 crosslinking agent does not modify this observation.



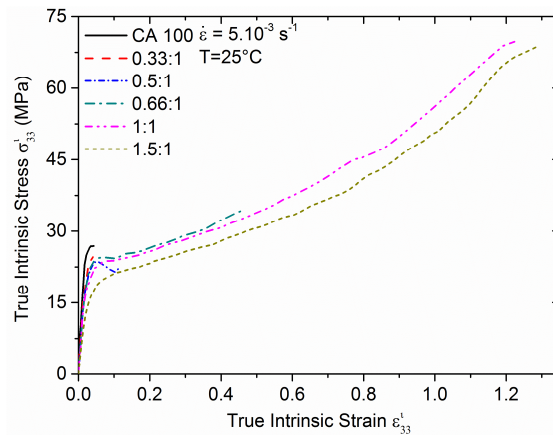
444 **Fig. 10.** Evolution of the fracture surfaces of a) unmodified CA 100, b) 0.5:1, c) 1:1,  
 445 and d) 1.5:1 materials by SEM micrographies.  
 446

447 To take in consideration the difference of volume strain level between the materials and to  
 448 compare the real mechanical behavior of all the materials at high values of true strain, the  
 449 intrinsic true mechanical behaviors were determined as developed in a previous paper [18]. The  
 450 shape of cavities was estimated to be tube-like shaped. This way, the intrinsic true strain in the  
 451 axial direction and the intrinsic true stress are given by:

$$452 \quad \varepsilon_{33}^i = \varepsilon_{33} \quad (14)$$

$$453 \quad \sigma_{33}^i = \frac{F}{S^i} = \sigma_{33} \frac{S}{S^i} = \sigma_{33} e^{\varepsilon_v} \quad (15)$$

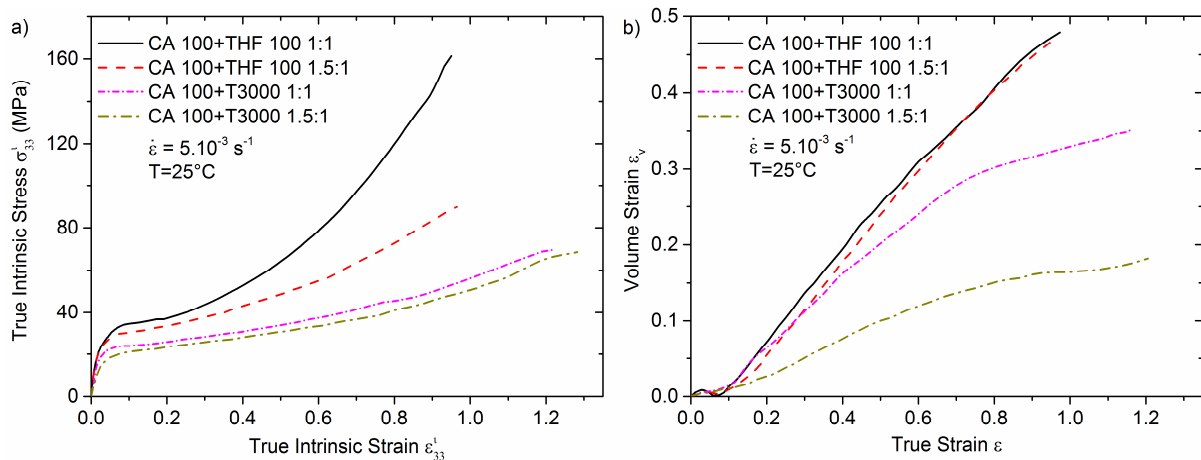
454 As a result, Fig. 11 presents the intrinsic true mechanical behaviours of the different materials.  
 455 Thanks to this correction of the volume strain the mechanical resistance increases as a function  
 456 of the amine/MAH molar ratio, with a maximum for the 1:1 material. It is interesting to look at  
 457 the evolution between the 1:1 and 1.5:1 material. Both material present close intrinsic true  
 458 mechanical behaviours, but at equal true strain the 1:1 material presents the higher level of true  
 459 stress. The plasticizing effect of the unreacted amino groups is here again put in evidence.



460  
461

**Fig. 11.** True intrinsic mechanical behaviours of the different materials as function of the NH<sub>2</sub>:MAH molar ratio.

462 Finally, to compare the effects of two crosslinking agents that differs in terms of geometry, the  
 463 polyether diamine and the polyether triamine, the intrinsic true mechanical behaviours and the  
 464 volume strain evolutions for both agents at the 1:1 and 1.5 molar ratios are given in Fig. 12.  
 465 The two crosslinking agents impact the mechanical behaviour with the switch from brittle to  
 466 ductile, but not with the same final properties. Indeed, the materials modified with the THF 100  
 467 (linear polyether diamine [20]) show higher intrinsic true stress level and higher volume strain  
 468 level, but the T3000 materials present higher intrinsic true strain at break, and a lower impact  
 469 of the excess of amino groups on the intrinsic properties. In addition, the T3000 materials show  
 470 a high impact of the excess of amine on volume strain level. In conclusion, with the same  
 471 reaction but with different molecular structure, different mechanical properties are reached.



472  
473  
474

**Fig. 12.** Comparison of the a) true intrinsic mechanical behaviour and b) volume strain evolution for the crosslinked materials with the two polyether amines in the cases of 1:1 and 1.5:1 molar ratios.

475

## 476 **Conclusion:**

477 The *in situ* crosslinking reaction performed by twin-screw extrusion on the iPP-g-MAH by the  
 478 Jeffamine™ polyether triamine T3000 was confirmed by the infrared spectroscopy and gel  
 479 content determination, and the 3D network appears more complex compared with the one  
 480 obtained by using linear diamine [20]. A slight nucleating effect is observed for the low molar  
 481 ratio (0.33:1) but is counterbalanced for higher molar ratios with a small decrease of the  
 482 crystalline lamellae thickness. This modification is shown by the fall of the main melting  
 483 temperature and the crystallisation of smallest iPP macromolecular elements. The crosslinked

484 network is maximal for the equimolar ratio. It induces an increase of stiffness of the matrix, as  
485 seen with the Brillouin spectroscopy results and more importantly, a switch of mechanical  
486 behavior from brittle to ductile. This switch starts to appear with the 0.33:1 molar ratio and the  
487 best mechanical properties are obtained for the 1:1. The 1.5:1 material shows that the excess of  
488 triamine induces a slight decrease of the elastic modulus and the volume strain, but presents  
489 finally a very close true mechanical behavior in comparison to the one obtained for the 1:1  
490 material.

491 Compared with the same initial material crosslinked with polyether diamine [20], the polyether  
492 triamine materials present a highest true strain level at break, and lower level of volume strain  
493 and true intrinsic stress, as revealed by VidéoTraction™. An interesting result is that the impact  
494 of the polyether triamine excess, on the 1.5:1 molar ratio material, is less important compared  
495 with the polyether diamine at the same molar ratio. Statistically, in this situation, two of the  
496 three amine groups of each T3000 molecules react with different MAH groups from the CA  
497 100 and maintained the 3D network, with remaining free NH<sub>2</sub> groups. The other interesting  
498 material is the 0.66:1 molar ratio, which exhibits an important rise of the mechanical properties,  
499 with remaining MAH groups for further reaction.

500 Such materials show interesting level of ductility and volume strain (essential to ensure good  
501 shock absorption properties) and remaining MAH or NH<sub>2</sub> groups grafted to the matrix. As  
502 described before, different techniques are used to obtain functionalized polyolefin with free  
503 MAH or amine groups, but such materials present low mechanical properties compared to those  
504 new materials.

505

## 506 **Acknowledgements**

507 The authors thank Huntsman, Eastman and Arkema for providing chemicals and  
508 polymers and Provisys Engineering Company for facilities with the VidéoTraction™  
509 system. AL and MP thank the French Ministry for the PhD grant and the LabEX  
510 DAMAS for the financial support.

511

## 512 **References**

513 [1] Q.W. Lu, C.W. Macosko, J. Horrión, J. of Polym. Sci., Part A: Polym. Chem. 43 (2005)  
514 4217–4232.

515 [2] A. Colbeaux, F. Fenouillot, J.F. Gerard, M. Taha, H. Wautier, Polym. Inter. 54 (2005)  
516 692–697.

517 [3] F.P. Tseng, J.J. Lin, Polymer. 42 (2001) 713–725.

518 [4] M. Hsiao, S. Liao, Y. Lin, C. Wang, N. Pu, H. Tsai, C.M. Ma, Nanoscale. 3 (2011)  
519 1516–1522.

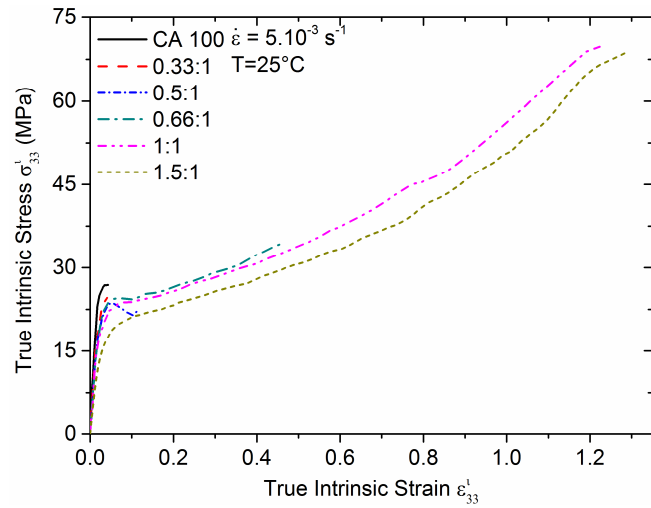
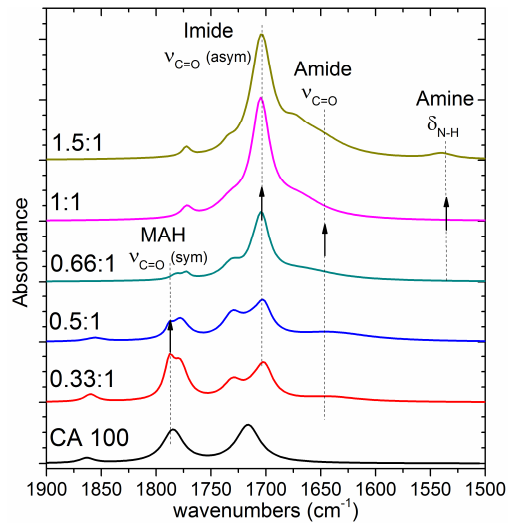
520 [5] X. Li, P. Bandyopadhyay, T.T. Nguyen, O. Park, J.H. Lee, J. of Membr. Sci. 47 (2018)  
521 80–92.

522 [6] R.A. Shanks, F.T. Cerezo, Composites: Part A. 43 (2012) 1092–1100.

- 523 [7] Y. Minoura, M. Ueda, S. Mizunuma, M. Oba, *J. of Appl. Polym. Sci.* 13 (1969) 1625–  
524 1640.
- 525 [8] R.M. Ho, A.C. Su, C.H. Wu, S.I. Chen, *Polymer* 34 (1993) 3264–3269.
- 526 [9] R. Zhang, Y. Zhu, J. Zhang, W. Jiang, J. Yin, *J. Polym. Sci., Part A-1: Polym. Chem.*,  
527 43 (2005) 5529–5534.
- 528 [10] S.H.P. Bettini, J.A.M. Agnelli, *J. Appl. Polym. Sci.* 85 (2002) 2706–2717.
- 529 [11] K. Cao, Z. Shen, Z. Yao, B. Qu, X. Pang, Z. Lu, et al., *Chem. Eng. Sci.* 65 (2010) 1621–  
530 1626.
- 531 [12] R. Rengarajan, V.R. Parameswaran, M. Vicic, S. Lee, P.L. Rinaldi, *Polymer* 31(1990)  
532 1703–1706.
- 533 [13] V. Khunova, Z. Zamorsky, *Polym. Plast. Technol. Eng.* 32 (1993) 289–296.
- 534 [14] J.M. Garcia-Martinez, O. Laguna, E.P. Collar, *J. Appl. Polym. Sci.* 68 (1998) 483–495.
- 535 [15] F. Ide, A. Hasegawa, *J. Appl. Polym. Sci.* 18 (1974) 963–974.
- 536 [16] M.F. Diop, J.M. Torkelson, *Polymer* 54 (2013) 4143–4154.
- 537 [17] D. Shi, J. Yang, Z. Yao, Y. Wang, H. Huang, W. Jing, et al., *Polymer* 42 (2001) 5549–  
538 5557.
- 539 [18] M. Ponçot, F. Addiego, A. Dahoun, *Int. J. Plast.* 40 (2013) 126–139.
- 540 [19] L. Cui, D.R. Paul, *Polymer* 48 (2007) 1632–1640.
- 541 [20] A. Létoffé, S.M. García-Rodríguez, S. Hoppe, N. Canilho, O. Godard, A. Pasc, I.  
542 Royaud, M. Ponçot, *Polymer* 164 (2019) 67–78.
- 543 [21] A.R. Padwa, Y. Sasaki, K.A. Wolske, C.W. Macosko, *J. Polym. Sci. 1 Polym. Chem.*  
544 33 (1995) 2165–2174.
- 545 [22] K.Y. Kim, S.C. Kim, *Macromol. Symp.* 214 (2004) 289–297.
- 546 [23] Jeffamines® Polyetheramines, Technical Specifications Sheet by Hunstman.
- 547 [24] Orevac® CA100, Technical Specifications Sheet by Arkema.
- 548 [25] P.H. Hermans, A. Weidinger, *J. Appl. Phys.* 19 (1948) 491–506.
- 549 [26] Z. Bartczak, A. Galeski, A.S. Argon, R.E. Cohen, *Polymer* 37 (1996) 2113–2123.
- 550 [27] M. Kakudo, N. Kasai, *X-ray Diffraction by Polymers*, Kodansha Ltd, Tokyo, Japan,  
551 1972.
- 552 [28] B. Wunderlich, *Macromolecular physics, Crystal Melting*, vol. 3, Academic Press, New  
553 York, 1980.
- 554 [29] D.C. Bassett, R.H. Olley, *Polymer* 25 (1984) 935–943.
- 555 [30] A.J. Müller, Z.H. Hernandez, M.L. Arnal, J.J. Sanchez, *Polym. Bull.* 39 (1997) 465–  
556 472.

- 557 [31] M.L. Arnal, V. Balsamo, G. Ronca, A. Sanchez, A.J. Müller, E. Canizales, et al., J.  
558 Therm. Anal. Calorim. 59 (2000) 451–470.
- 559 [32] A.J. Müller, R.M. Michell, R.A. Pérez, A.T. Lorenzo, Eur. Polym. J. 65 (2015) 132–  
560 154.
- 561 [33] S. Ogier, C. Vidal, D. Chapron, P. Bourson, I. Royaud, M. Ponçot, et al., J. Polym.  
562 Sci., Part B: Polym. Phys. 55 (2017) 866–876.
- 563 [34] C. G'Sell, J.M. Hiver, A. Dahoun, A. Souahi, J. Mater. Sci. 27 (1992) 5031–5039.
- 564 [35] F. Addiego, A. Dahoun, C. G'Sell, J.M. Hiver, Polymer 47 (2006) 4387–4399.
- 565 [36] C. G'Sell, J.M. Hiver, A. Dahoun, Int. J. Solid Struct. 39 (2002) 3857–3872.
- 566 [37] M. Ponçot, PhD Thesis, INPL-ENSMN, Nancy, France, 2009.
- 567 [38] C.B. Bucknall, D. Clayton, W. Keast, J. Mater. Sci. 8 (1973) 514–524.
- 568 [39] S.I. Naqui, I.M. Robinson, J. Mater. Sci. 28 (1993) 1421–1429.
- 569 [40] B. Pukánszky, M. Vanes, F.H.J. Maurr, G. Vörös, J. Mater. Sci. 29 (1994) 2350–2358.
- 570 [41] N. Billon, Mec. Ind. 4 (2003) 357–364.
- 571 [42] J. Ye, PhD Thesis, Lorraine University – LEMTA, Nancy, France, 2015.
- 572 [43] J. K. Krüger, Brillouin Spectroscopy and its Application to Polymers. HEINZ, B. (ed.)  
573 Optical Techniques to Characterize Polymer Systems. Amsterdam: Elsevier, (1989).
- 574 [44] D. Rouxel, C. Thevenot, V.S. Nguyen, B. Vincent, Brillouin spectroscopy of polymer  
575 nanocomposites, Spectroscopy of Polymer Nanocomposites, pp362-392, ISBN:  
576 9780323401838 Elsevier (2016).
- 577 [45] B. Vincent, J. K. Krüger, O. Elmazria, L. Bouvot, R. Sanctuary, D. Rouxel, P. Alnot,  
578 J. of Phys. D: Appl. Phys. 38 (2005) 2026-2030.
- 579 [46] R. Bactavatchalou, P. Alnot, J. Bailer, M. Kolle, U. Müller, M. Philipp, W. Possart, D.  
580 Rouxel, R. Sanctuary, A. Tschöpe, C. Vergnat, B. Wetzler, J. K. Krüger 40 (2006) 111-117.
- 581 [47] J. K. Krüger, U. Müller, R. Bactavatchalou, D. Liebschner, M. Sander, W. Possart, C.  
582 Wehlack, J. Baller, D. Rouxel, Mechanical Interphases in Epoxies as seen by Nondestructive  
583 High-Performance Brillouin Microscopy. POSSART, W. (ed.) Adhesion. Wiley-VCH Verlag  
584 GmbH & Co. KGaA, 2005.
- 585 [48] V.S. Nguyen, D. Rouxel, M. Meier, B. Vincent, A. Dahoun, S. Thomas, F.D. Dos  
586 Santos, Pol. Eng. and Sci. 54 (2014) 1280-1288.
- 587 [49] D. Rouxel, J. Eschbach, B. Vincent, Int. J. of Surf. Sci. and Eng. 4 (2010) 322-336.
- 588 [50] G. Maurice, D. Rouxel, B. Vincent., R. Hadji, J.F. Schmitt, B. Taghite, R. Rahouadj,  
589 Polym. Eng. Sci. 53 (2013) 1502-1511.
- 590 [51] R. Hadji, V.S. Nguyen, B. Vincent, D. Rouxel, F. Bauer, Ieee Transactions on  
591 Ultrasonics Ferroelectrics and Frequency Control 59 (2012) 163-167.

- 592 [52] B. Vigolo, B. Vincent, J. Eschbach, P. Bourson, J.F. Mareche, E. Mcrae, A. Muller, A.  
593 Soldatov, J.M. Hiver, A. Dahoun, D. Rouxel, *J. Phy. Chem. C* 113 (2009) 17648-17654.
- 594 [53] S. Rouabah, B. Vincent, A. Chaabi, D. Rouxel, S. Girard, *Eur. Phys. J. Appl. Phys.*,  
595 Volume 77, Issue: 3 (2017) 30701.
- 596 [54] G. Turner-Jones, P. Corradini, *Il Nuovo Cimento* 15 (1960) 40–51.
- 597 [55] A. Turner-Jones, A.J. Cobbold, *J. Polym. Sci. art C: Polym. Lett.* 6 (1968) 539–546.
- 598 [56] S. Bouhelal, M.E. Cagiao, D. Benachour, F.J. Baltá Calleja, *J. Appl. Polym. Sci.* 103  
599 (2007) 2968–2976.
- 600 [57] S. Bouhelal, M.E. Cagiao, S. Khellaf, H. Tabet, B. Djellouli, D. Benachour, et al., *J.*  
601 *Appl. Polym. Sci.* 115 (2010) 2654–2662.
- 602 [58] Z. Song, W.E. Baker, *J. Polym. Sci. 1 Polym. Chem.* 30 (1992) 1589–1600.
- 603 [59] F. Muñoz, A. Saitohb, R. J. Jiménez-Riobóo, R. Balda, *J. of Non-Crystal. Sol.* 473  
604 (2017) 125–131.



From the 0.66:1 NH<sub>2</sub>/MAH molar ratio, crosslinking enables maleated isotactic polypropylene to get higher mechanical resilience while keeping its functional property with available free MAH or NH<sub>2</sub> grafts, confirmed by the FTIR analysis.